JTTEE5 24:136–143
DOI: 10.1007/s11666-014-0158-2
1059-9630/$19.00 © ASM International

Peer Reviewed

Synthesis and Phase Stability of Scandia, Gadolinia, and Ytterbia Co-doped Zirconia for Thermal Barrier Coating Application

Qi-Lian Li, Xiang-Zhong Cui, Shu-Qing Li, Wei-Hua Yang, Chun Wang, and Qian Cao

(Submitted June 2, 2014; in revised form August 30, 2014)

Scandia, gadolinia, and ytterbia co-doped zirconia (SGYZ) ceramic powder was synthesized by chemical co-precipitation and calcination processes for application in thermal barrier coatings to promote the durability of gas turbines. The ceramic powder was agglomerated and sintered at 1150 °C for 2 h, and the powder exhibited good flowability and apparent density to be suitable for plasma spraying process. The microstructure, morphology and phase stability of the powder and plasma-sprayed SGYZ coatings were analyzed by means of scanning electron microscope and x-ray diffraction. Thermal conductivity of plasma-sprayed SGYZ coatings was measured. The results indicated that the SGYZ ceramic powder and the coating exhibit excellent stability to retain single non-transformable tetragonal zirconia even after high temperature (1400 °C) exposure for 500 h and do not undergo a tetragonal-to-monoclinic phase transition upon cooling. Furthermore, the plasma-sprayed SGYZ coating also exhibits lower thermal conductivity than yttria stabilized zirconia coating currently used in gas turbine engine industry. SGYZ can be explored as a candidate material of ultra-high temperature thermal barrier coating for advanced gas turbine engines.

Keywords phase stability, scandia, gadolinia, and ytterbia co-doped zirconia, thermal barrier coatings

1. Introduction

Since superalloy components in hot sections of aircraft engine turbines operate close to the limits imposed by the onset of melting, thermal barrier coatings (TBCs) offer an attractive option to protect superalloy against the deleterious effects of high temperature turbine environments. Thermal barrier coating application results in considerable improvements in durability of hot section turbine components, as well as in an increase of gas turbine thermodynamic efficiency. The TBCs typically consist of a ceramic top coat deposited on the substrate with a metallic bond coat, which imparts oxidation protection to the substrate, and provides a surface to which the ceramic top coat can adhere well.

Yttria-stabilized zirconia with a composition of 3.5-4.5 mol%Y_2O_3-ZrO_2, here abbreviated as YSZ, ceramic deposits is often applied as top coat material for TBCs (Ref 1) YSZ coating can't be used for long-term above 1200 °C due to the destructive phase transformation of tetragonal phase to monoclinic phase which results in a significant change in volume of the coating and can cause cracking and rapid degradation of a TBC, especially under thermal cycling conditions Ref (2-4). In order to increase usage temperature of TBCs, it is very important that the TBCs structure should be designed to be ''phase non-transformable'' (Ref 5). The continual increase in gas turbine inlet temperatures requires new TBCs material with improved phase stability and reduced thermal conductivity.

In recent years, the rare earth oxides (Yb_2O_3, Sc_2O_3, Gd_2O_3, La_2O_3,Y_2O_3 et al.) as co-dopants of ZrO_2 have been widely investigated (Ref 5-11). Some rare-earth zirconates with low thermal conductivity, such as $La_2Zr_2O_7$, $Gd_2Ce_2O_7$, $La_2(Zr_{0.7}Ce_{0.3})_2O_7$, were also explored (Ref 12-16). Before this paper, some compositions of Sc_2O_3-Gd_2O_3-Yb_2O_3-ZrO_2 had been prepared and tested in our laboratory. In this experiment, a new composition of 5.5 mol%Sc_2O_3-2.0 mol%Gd_2O_3-2.0 mol%Yb_2O_3-ZrO_2, here abbreviated as SGYZ, was designed and the powder material was synthesized by chemical co-precipitation method. The SGYZ coatings were deposited by plasma spraying and subjected to anneal at 1400 °C for 500 h. The phase stability and thermal conductivity of the SGYZ coating were examined and compared with YSZ

This article is an invited paper selected from presentations at the 2014 International Thermal Spray Conference, held May 21-23, 2014, in Barcelona, Spain, and has been expanded from the original presentation.

Qi-Lian Li, Xiang-Zhong Cui, Shu-Qing Li, Wei-Hua Yang, Chun Wang, and **Qian Cao**, Science and Technology on Power Beam Processes Laboratory, Beijing Aeronautical Manufacturing Technology Research Institute, Chaoyang District 100024, Beijing, China. Contact e-mail: qilian1818@sina.com.

coating in order to evaluate the effects of Sc_2O_3, Gd_2O_3 and Yb_2O_3 and possibility of developing 5.5 mol%Sc_2O_3-2.0 mol%Gd_2O_3-2.0 mol%Yb_2O_3-ZrO_2 as a ceramic top coating material for TBCs.

2. Experimental

2.1 Powder Synthesis and Characterizations

Scandia, gadolinia, and ytterbia powders were chosen as starting materials. They were dissolved into a certain amount of hydrochloric acid solution to prepare Sc^{3+}, Gd^{3+} and Yb^{3+} salt solutions, respectively. Zirconium oxychloride was dissolved into de-ionized water. They were mixed in the appropriate proportion to produce a precursor solution for a desired composition of 5.5 mol%Sc_2O_3-2.0 mol%Gd_2O_3-2.0 mol%Yb_2O_3-ZrO_2. The precursor solution was slowly added to a 4 M NH_4OH solution and reacted with it at pH >11 to produce a precipitate. The precipitate was filtered and washed with de-ionized water to drive out impure ions. Then the washed precipitate was dried in an oven at 200 °C for 12 h to obtain the precursor powder. Finally, SGYZ initial powder was obtained by calcining the precursor powder at 850 °C for 24 h, with a grain size of about 100 nm. The compositions of the SGYZ initial powder were analyzed by inductively coupled plasma-atomic emission spectrometer (ICP-AES), as shown in Table 1.

The SGYZ initial powder was mixed with water, a dispersing agent (polyethylene glycol 2000) and a binder (polyvinyl alcohol 1788) in an agitator for 4 h. Afterward, the slurry was well de-agglomerated in an attrition mill for 2 h. Then the slurry was spray-dried and agglomerated. The SGYZ powder for plasma spraying thermal barrier coating application was obtained by agglomerating the initial powder into spherical micrometer-size granules (20-60 μm) and sintering it at 1150 °C for 2 h. During sintering, organic dispersing agent and binder were all removed.

The morphology of the SGYZ initial powder is shown in Fig. 1. SEM magnified image of the SGYZ initial powder is shown in Fig. 2. The appearance of agglomerated and sintered SGYZ powder for plasma spraying is shown in Fig. 3, and the SEM magnified image for the surface of plasma spraying powder is shown in Fig. 4. From Fig. 2 and 4, it can be seen that the grain size of both SGYZ initial powder and agglomerated powder is about 100 nm.

Furthermore, the flowability and apparent density were measured. The flowability of agglomerated and sintered SGYZ was 34 s/50 g and the apparent density

Table 1 Chemical compositions of the SGYZ initial powder

Oxides	Sc_2O_3	Gd_2O_3	Yb_2O_3	ZrO_2
mol%	5.46	1.98	1.96	90.6

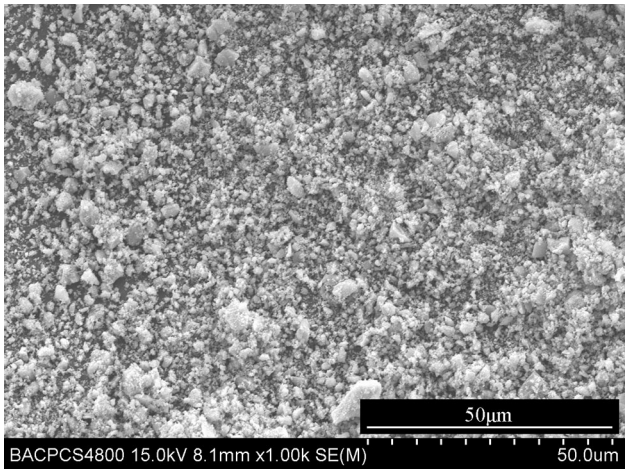

Fig. 1 SEM micrograph of the SGYZ initial powder

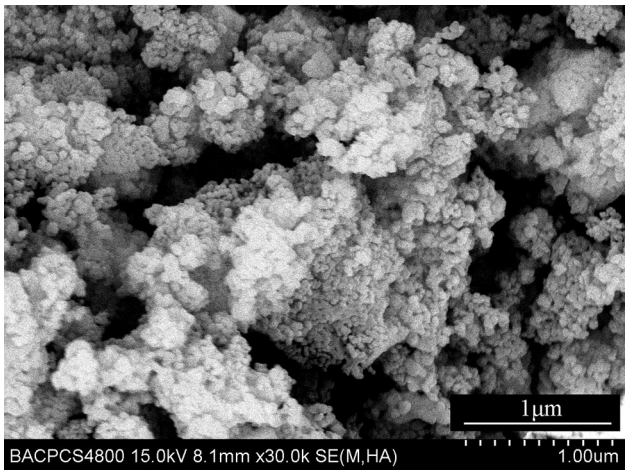

Fig. 2 SEM magnified image of the SGYZ initial powder

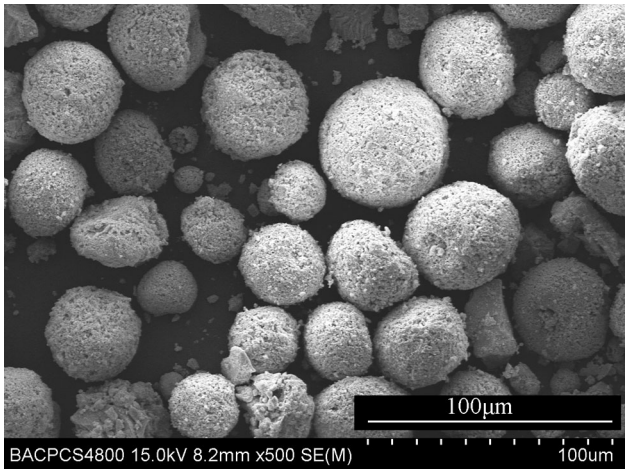

Fig. 3 Appearance of agglomerated and sintered SGYZ powder

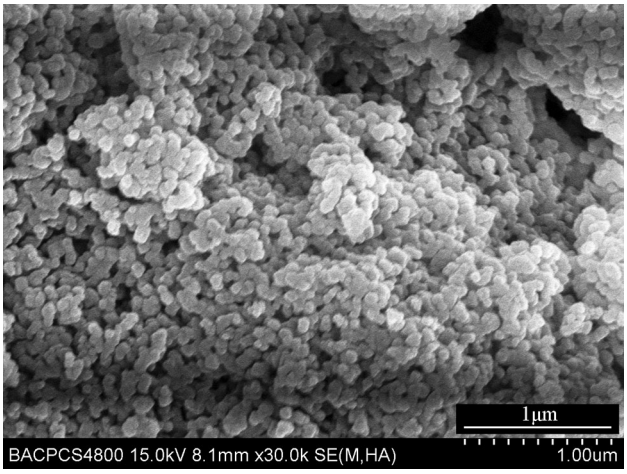

Fig. 4 SEM magnified image of agglomerated and sintered SGYZ powder surface

Table 2 Plasma spraying parameters, with A3000 plasma spray system

Parameters	NiCrAlYSi	SGYZ,YSZ
Current, A	500	600
Voltage, V	70	75
Primary gas Ar, SLPM	60	40
Secondary gas H_2, SLPM	7	12
Carrier gas Ar, SLPM	4	4
Powder feed rate, g/min	40	30
Spray distance, mm	150	70
Traverse speed of torch, mm/s	400	400

was 1.85 g/cm^3, which were very suitable for plasma spraying process.

2.2 Plasma Spraying Process

NiCrAlYSi metallic bond coating and 5.5 mol%Sc_2O_3-2.0 mol%Gd_2O_3-2.0 mol%Yb_2O_3-ZrO_2 ceramic top coating were deposited on Ni_3Al-based superalloy substrates with A3000 plasma spray system. Before spraying, Ni_3Al-based superalloy specimens were grit blasted with brown corundum to a surface roughness Ra of about 10 μm. The thickness the bond coating was about 0.1 mm, and the thickness of the ceramic top coating was about 0.25 mm. Table 2 provides the plasma spray conditions for the coatings under study, using an A3000 atmospheric plasma spray system supplied by Sulzer Metco. Figure 5 illustrates the microstructure of SGYZ coating with a NiCrAlYSi metallic bond coating on a Ni_3Al-based superalloy substrate.

In order to prepare the coating samples for phase stability assessment and thermal conductivity measurement, SGYZ(5.5 mol%Sc_2O_3-2.0 mol%Gd_2O_3-2.0 mol%Yb_2O_3-ZrO_2) and YSZ (4.5 mol%Y_2O_3-ZrO_2) powders were plasma sprayed onto an aluminum plate substrate with grooves (Φ12.7 mm × 1 mm). The ceramic coatings without NiCrAlYSi metallic bond coatings were deposited full of the grooves, the ceramic coatings were stripped off from

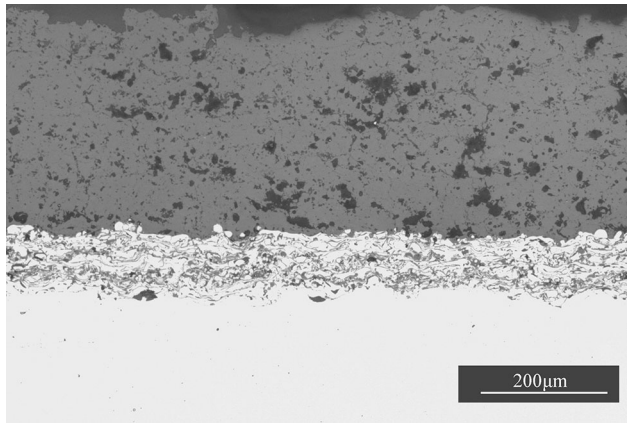

Fig. 5 A metallographic cross section of the SGYZ coating with a bond coating

aluminum substrate using 50/50 NaOH-H_2O solution. The detached coating samples with a dimension of Φ12.7 mm × 1 mm were obtained for the measurements of phase stability and thermal conductivity.

2.3 Phase Stability

For the phase stability assessment, the SGYZ powder and coating were heat-treated at 1400 °C for 300 and 500 h, but for YSZ coating at 1400 °C for 100 and 300 h. The phase structures were determined by x-ray diffraction technique (D8 advance), and the radiation source was Ni filtered with Cu Kα, λ=0.1542 nm. For each sample, x-ray diffraction was performed in a step-scan mode with an angle increment of 0.02° in the diffraction angle 2θ from 20° to 80°. The x-ray diffraction peak identification, 2θ values at peaks, peak integral net intensity and cell parameters were performed using Jade 5.0 software package (Material Data Incorporated). The mole percents of monoclinic phase M_m, tetragonal phase $M_{t/t'}$ and cubic phase M_c were determined from the most common equation (Ref 17, 18):

$$\frac{M_m}{M_{c,t/t'}} = 0.82\frac{I_m(\bar{1}11) + I_m(111)}{I_{c,t/t'}(111)} \quad \text{(Eq 1)}$$

$$\frac{M_c}{M_{t/t'}} = 0.88\frac{I_c(400)}{I_{t/t'}(004) + I_{t/t'}(400)} \quad \text{(Eq 2)}$$

where I_m ($\bar{1}$ 11) and I_m(111) are the integral net intensities for monoclinic phase reflected from ($\bar{1}$ 11) and (111) peaks, respectively. $I_{c,t/t'}$(111) is the intensity for cubic and tetragonal phase reflected from (111) plane. I_c(400) is the intensity for cubic phase reflected from (400) plane. $I_{t/t'}$(004) and $I_{t/t'}$(400) are the intensities for tetragonal phase reflected from (004) and (400) plane, respectively.

2.4 Thermal Conductivity

The measurements of thermo-physical properties were carried out on the samples with 12.7 mm in diameter and 1 mm in thickness and the temperature ranges from 500 to

1600 °C. Thermal conductivity λ (W/m K) is calculated from:

$$\lambda = \alpha C_p \rho \quad \text{(Eq 3)}$$

where ρ is the density (kg/m^3), C_p is the specific heat capacity (J/kg K), and α is the thermal diffusivity (m^2/s).

The specific heat capacity (C_p) was measured by laser radiation method. When the laser beam was projected over the full face of the specimen, one part of the energy was absorbed by the sample and the other part was radiated reflecting by a detector. The rising temperature of the rear face of the sample was measured and the specific heat capacity C_p was calculated based on the following equation:

$$C_p = \frac{E_{Pro} - E_{Ra}}{M(T_2 - T_1)} = \frac{E_{Ab}}{M(T_2 - T_1)} = \frac{E_{Ab}}{M\Delta T} \quad \text{(Eq 4)}$$

where M is the mass of the sample, E_{Pro} is the project energy of the laser beam, E_{Ra} is the energy radiated reflecting by the detector, E_{Ab} is the energy absorbed by the sample, T_1 and T_2 are the temperatures of rear face before and after laser projecting, respectively.

The thermal diffusivity (α), as a function of temperature was measured using a laser flash technique (Ref 19). The density (ρ) was measured by Archimedes' method.

Because the coating samples were not fully dense, the measured thermal conductivity λ for the ceramic coatings can be modified for the fully dense ceramic sample λ_o using following equation (Ref 20):

$$\lambda / \lambda_o = 1 - 4\Phi/3 \quad \text{(Eq 5)}$$

where Φ is the fraction of porosity inside the coating sample which was determined using the relationship $\Phi = 1 - \rho/\rho_t$, where ρ_t is the theoretical density of the fully dense ceramic sample, and ρ is the measured density of the ceramic coating. In this paper, only the measured thermal conductivity λ for the SGYZ and YSZ ceramic coatings was discussed.

3. Results and Discussion

3.1 SGYZ and YSZ Powders

SGYZ composition was designed as 5.5 mol%Sc_2O_3-2.0 mol%Gd_2O_3-2.0 mol%Yb_2O_3-ZrO_2, and YSZ was prepared with a composition of 4.5 mol%Y_2O_3-ZrO_2. Figure 6 indicates that the XRD patterns of agglomerated and sintered SGYZ powder and YSZ powder are both coincident with the standard XRD spectrum of tetragonal ZrO_2. There are no diffraction peaks of Sc_2O_3, Gd_2O_3, Yb_2O_3 and Y_2O_3 observed in the powders, which means that Sc_2O_3, Gd_2O_3, Yb_2O_3 and Y_2O_3 have been dissolved in ZrO_2 crystal completely and stabilize ZrO_2 by substituting Sc^{3+}, Gd^{3+}, Yb^{3+} and Y^{3+} for Zr^{4+}. From the {111} diffraction region no monoclinic phase is observed for both SGYZ and YSZ powders.

3.2 Phase Stability of the SGYZ and YSZ Coatings

The phase structures of as-sprayed YSZ coating and the YSZ coating after a heat treatment of 100 and 300 h at 1400 °C are presented in Fig. 7. According to literature (Ref 21), the appearance of monoclinic m phase in the annealed YSZ coating arose from the partitioning of the non-transformable tetragonal t′ phase to the equilibrium tetragonal t phase and cubic c phase during high temperature annealing. The equilibrium tetragonal t phase then transformed to monoclinic m phase during the cooling process. The non-transformable tetragonal t′ phase and transformable t phase can be distinguished by the tetrag-

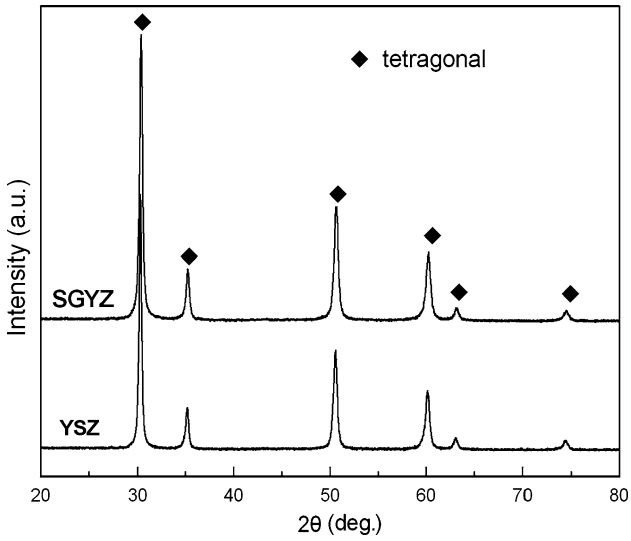

Fig. 6 XRD patterns of SGYZ and YSZ powders

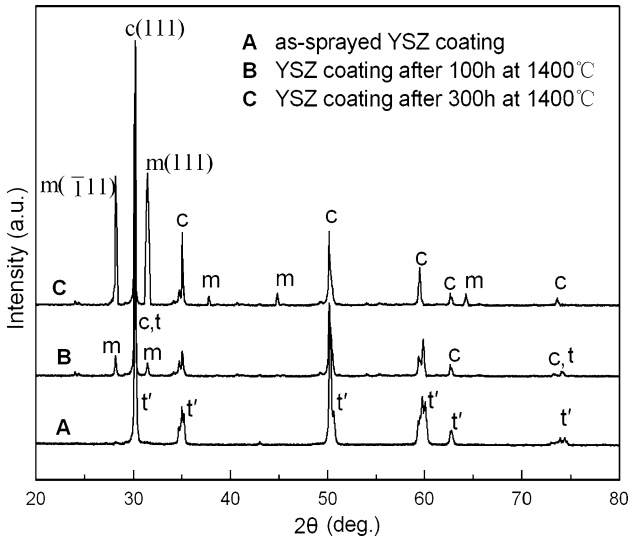

Fig. 7 XRD patterns of as-sprayed YSZ coating and the coating after a heat treatment of 100 and 300 h at 1400 °C

onality 'c/$\sqrt{2}$ a'. The ratio tends to be less than 1.010 for the t′ phase while it is superior to 1.010 for t phase (Ref 21). Figure 8 and 9 indicate {111} and {400} peaks regions of the YSZ coating after a heat treatment of 100 h at 1400 °C, respectively. The diffraction peaks of monoclinic {111} can be seen clearly, and cubic (400) peak appears between tetragonal (004) and (400) peaks. All these indicate that partial tetragonal phase has transformed to monoclinic m phase in YSZ during annealing at 1400 °C for 100 h and sequent cooling. According to calculation by Eq 1 and 2, the amounts of monoclinic, cubic and tetragonal phase are of 23.2,27.1 and 49.7 mol%, respectively. The tetragonality 'c/$\sqrt{2}$ a' equals to 1.0163, so the tetragonal phase is t phase.

Phase compositions, cell parameters and tetragonality 'c/$\sqrt{2}$ a' for YSZ and SGYZ coatings are given in Table 3. It can be seen that the YSZ coating after a heat treatment of 300 h at 1400 °C was composed of cubic c phase and monoclinic m phase and the content of monoclinic m phase is about 48.7 mol% calculated by Eq 1, which means that tetragonal phase in YSZ was essentially converted to the monoclinic m phase and cubic c phase under 1400 °C annealing for 300 h and sequent cooling. No tetragonal t or t′ phase is detected in the annealed YSZ coating for 300 h at 1400 °C, which also confirms that YSZ thermal barrier coating lacks ultra-high temperature phase stability.

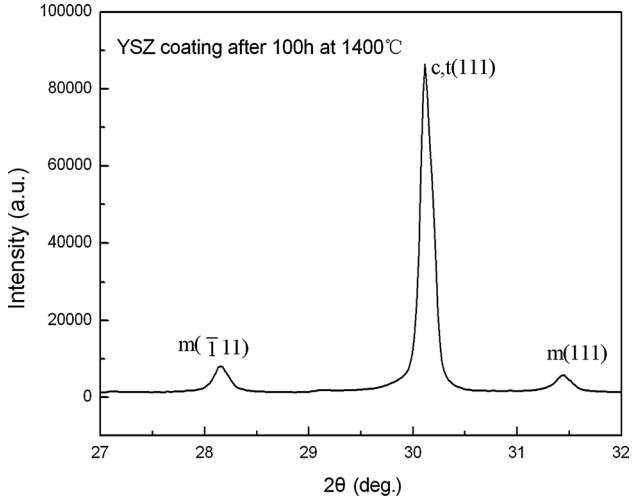

Fig. 8 XRD {111} peaks of YSZ coating after a heat treatment of 100 h at 1400 °C

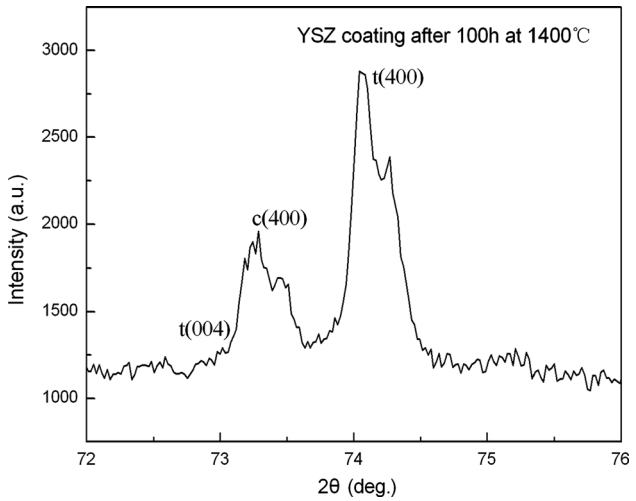

Fig. 9 XRD{400} peaks of YSZ coating after a heat treatment of 100 h at 1400 °C

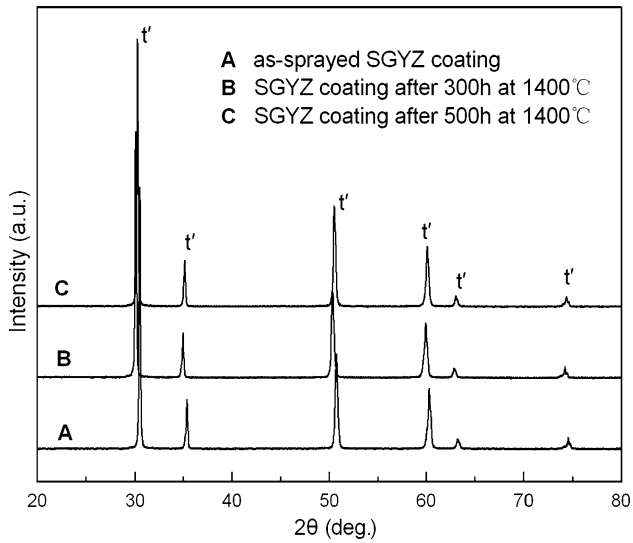

Fig. 10 XRD patterns of as-sprayed SGYZ coating and the coatings after a heat treatment of 300 and 500 h at 1400 °C

Table 3 Phase compositions, cell parameters and tetragonality c/$\sqrt{2}$ a

Coatings	Treatment	Phase composition	Cell parameter, nm	c/$\sqrt{2}$ a
YSZ	As-sprayed	100 mol% t′	$a=b$=0.36046 c=0.51393	1.0082
	1400 °C 100 h	49.7 mol% t	$a=b$=0.35918 c=0.51623	1.0163
		27.1 mol% c	$a=b=c$=0.51342	…
		23.2 mol% m	a=0.51312 b=0.52205 c=0.53608	…
	1400 °C 300 h	51.3 mol% c	$a=b=c$=0.51273	…
		48.7 mol% m	a=0.51607 b=0.51968 c=0.53106	…
SGYZ	As-sprayed	100 mol% t′	$a=b$=0.35976 c=0.51129	1.0049
	1400 °C 300 h	100 mol% t′	$a=b$=0.36028 c=0.51176	1.0044
	1400 °C 500 h	100 mol% t′	$a=b$=0.35982 c=0.51278	1.0077

For SGYZ coatings, no evidence of monoclinic m phase and cubic c phase was found but single tetragonal phase remained after a heat treatment of 300 or 500 h at 1400 °C as shown in Fig. 10, 11 and 12. After a heat treatment of 500 h at 1400 °C, the tetragonality 'c/$\sqrt{2}$ a' equals to 1.0077 (less than 1.010), so the tetragonal phase in the annealed SGYZ is still t′ phase, which confirms 1400 °C phase stability of tetragonal phase in the zirconia stabilized with a indicated composition of scandia, gadolinia, and ytterbia.

According to kinetic consideration, the partitioning of t′ phase to equilibrium t phase and c phase during high-temperature annealing is diffusion controlled and requires long-range cations diffusion. But the t′ phase stability depends not only on the diffusion kinetics but also on the driving force for partitioning of t′ (Ref 22, 23). More subsequent experiments for the SGYZ coatings will be needed in order to explain that the phase stability of SGYZ is much better in comparison with YSZ.

3.3 Thermal Conductivity

As shown in Fig. 13, 14 and 15, the thermal diffusivity, the specific heat capacity and the thermal conductivity of the SGYZ coating are all lower than that of YSZ coating, respectively, in the measured temperature range from 500 to 1600 °C. The reduction in the thermal conductivity is attributed to the addition of Sc_2O_3, Gd_2O_3 and Yb_2O_3, which introduce more volume fractions of point defects such as pores, oxygen vacancies and solute atoms.

It is known that the substitutional solid solution SGYZ is formed by the substitution of trivalent rare-earth cations (Sc^{3+}, Gd^{3+} or Yb^{3+}) for Zr^{4+} cations. The addition of low valency stabilizer ions has to introduce additional oxygen

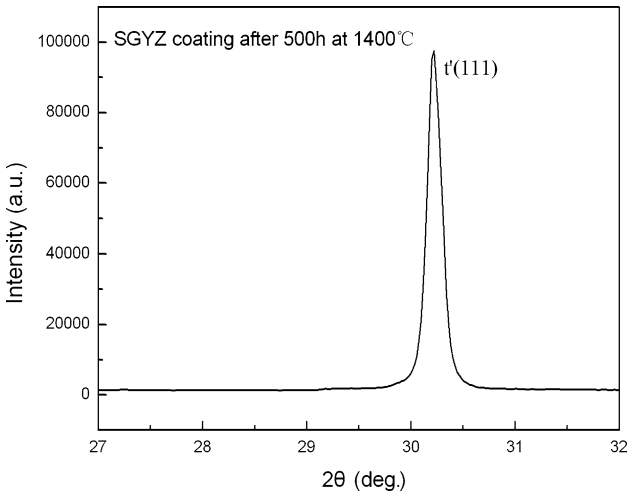

Fig. 11 XRD {111} peak of SGYZ coating after a heat treatment of 500 h at 1400 °C

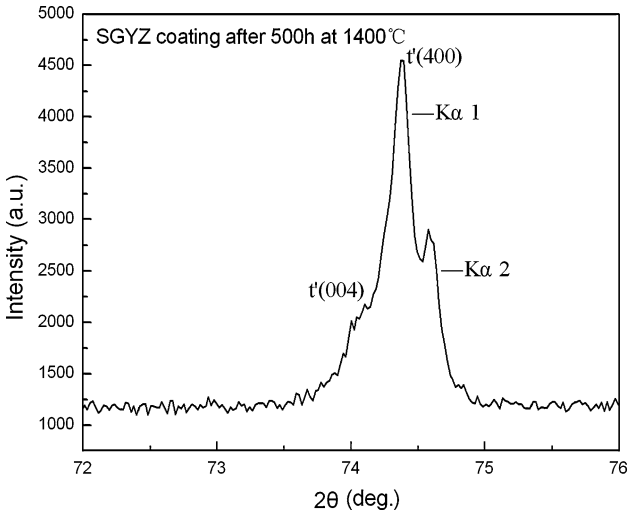

Fig. 12 XRD {400} peaks of SGYZ coating after a heat treatment of 500 h at 1400 °C

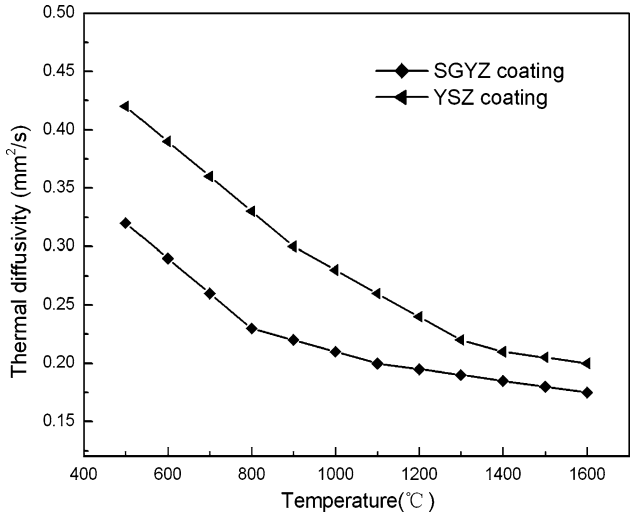

Fig. 13 Comparison of thermal diffusivity for SGYZ and YSZ coatings

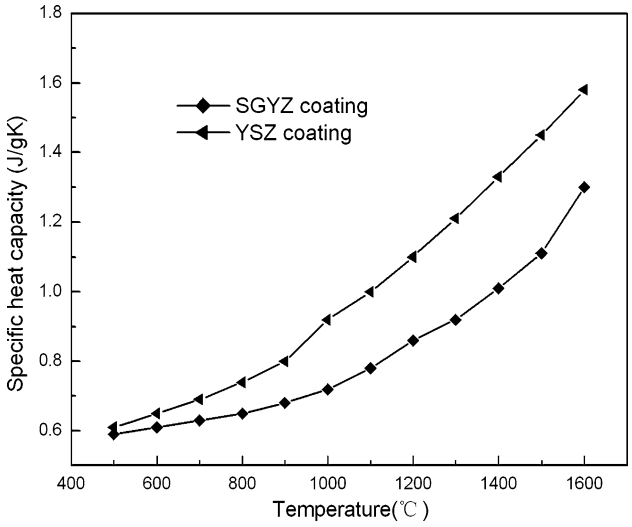

Fig. 14 Comparison of specific heat capacity for SGYZ and YSZ coatings

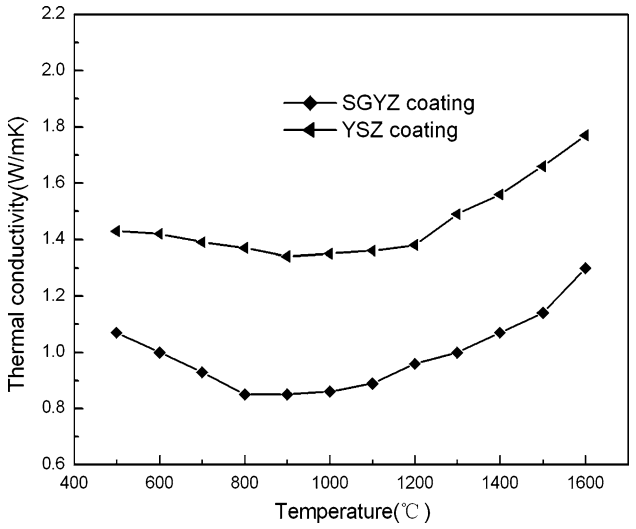

Fig. 15 Comparison of thermal conductivity for SGYZ and YSZ coatings

vacancies to maintain the electrical neutrality of the lattice. For SGYZ and YSZ, Sc^{3+}, Gd^{3+}, Yb^{3+} and Y^{3+} have the same valency and the total content of Sc_2O_3, Gd_2O_3 and Yb_2O_3 in SGYZ is 9.5 mol%, while the content of Y_2O_3 is only 4.5 mol% in YSZ. Clearly, the addition of Sc^{3+}, Gd^{3+} and Yb^{3+} in SGYZ creates more oxygen vacancies and substitutional point defects in comparison with YSZ. These defects can increase scattering of phonons and so reduce the thermal conductivity.

In this paper, the atomic weights of Sc, Gd,Yb, Y and Zr are 45, 157, 173, 89. and 91. respectively, and the ionic radiuses of Sc^{3+}, Gd^{3+}, Yb^{3+}, Y^{3+} and Zr^{4+} are 0.0732 nm, 0.0938 nm, 0.0858 nm, 0.0893 nm and 0.079 nm (Ref 24, 25). The atomic mass difference and the ionic radius difference between Sc and Zr are both greater than that between Y and Zr, maybe Sc_2O_3 has a much more significant effect on reducing thermal conductivity than Y_2O_3.

In this study, it can be concluded that 5.5 mol%Sc_2O_3-2.0 mol%Gd_2O_3-2.0 mol%Yb_2O_3-ZrO_2 ceramic material provides significant benefits for thermal barrier coating application due to its improved phase stability and reduced thermal conductivity in comparison with YSZ. The SGYZ may be a good choice for potential thermal barrier coating application at ultra-high temperature in the near future.

4. Conclusions

5.5 mol%Sc_2O_3-2.0 mol%Gd_2O_3-2.0 mol%Yb_2O_3-ZrO_2 (SGYZ) ceramic material offers remarkable opportunities for developing novel TBCs due to its improved phase stability. The SGYZ keeps single non-transformable tetragonal phase even after a heat treatment of 500 h at 1400 °C. Under the measurement range from 500 to 1600 °C, the thermal conductivity of SGYZ coating is lower than that of YSZ coating. SGYZ can be explored as a novel prospective candidate material for thermal barrier coating application.

References

1. X.Q. Cao, R. Vassen, and D. Stoever, Ceramic Materials for Thermal Barrier Coatings, *J. Alloys Compd.*, 2004, **24**, p 1-10
2. R.W. Trice, Y.J. Su, J.R. Mawdsley, K.T. Faber, A.R. De Arellano-Lopez, H. Wang, and W.D. Porter, Effect of Heat Treatment on Phase Stability, Microstructure and Thermal Conductivity of Plasma-Sprayed YSZ, *J. Mater. Sci.*, 2002, **37**(11), p 2359-2365
3. J. Ilavsky and J.K. Stalick, Phase Composition and Its Changes During Annealing of Plasma-Sprayed YSZ, *Surf. Coat. Technol.*, 2000, **127**(2-3), p 120-129
4. J. Moon, H. Choi, H. Kim, and C. Lee, The Effects of Heat Treatment on the Phase Transformation Behavior of Plasma-Sprayed Stabilized ZrO_2 Coatings, *Surf. Coat. Technol.*, 2002, **155**(1), p 1-10
5. M. Leoni, R.L. Jones, and P. Scardi, Phase Stability of Scandia-Yttria-Stabilized Zirconia TBCs, *Surf. Coat. Technol.*, 1998, **108-109**, p 107-113
6. M.N. Rahaman, J.R. Gross, R.E. Dutton, and H. Wang, Phase Stability, Sintering, and Thermal Conductivity of Plasma-Sprayed ZrO_2-Gd_2O_3 Composition for Potential Thermal Barrier Coating Applications, *Acta Mater.*, 2006, **54**, p 1615-1621
7. R.L. Jones, R.F. Reidy, and D. Mess, Scandia, Yttria-Stabilized Zirconia for Thermal Barrier Coatings, *Surf. Coat. Technol.*, 1996, **82**, p 70-75
8. R.L. Jones and D. Mess, Improved the Tetragonal Phase Stability at 1400 °C with Scandia, Yttria-Stabilized Zirconia, *Surf. Coat. Technol.*, 1996, **86-87**, p 94-101
9. M. Matsumoto, H. Takayama, D. Yokoe, K. Mukai, H. Matsubara, and Y. Kagiya, Thermal Cycle Behavior of Plasma Sprayed La_2O_3, Y_2O_3 Stabilized ZrO_2 Coatings, *Scr. Mater.*, 2006, **54**, p 2035-2039
10. M. Matsumoto, K. Aoyama, H. Matsubara, and H. Takayama, Thermal Conductivity and Phase Stability of Plasma Sprayed ZrO_2-Y_2O_3-La_2O_3 Coatings, *Surf. Coat. Technol.*, 2005, **194**, p 31-35
11. J.R. Brandon and R. Taylor, Phase Stability of Zirconia-Based Thermal Barrier Coatings, *Surf. Coat. Technol.*, 1991, **46**, p 75-90
12. X.Q. Cao, J.Y. Li, X.H. Zhong, J.F. Zhang, and Y.F. Zhang, R Vassen, $La_2(Zr_{0.7}Ce_{0.3})_2O_7$—A New Oxide Ceramic Material with High Sintering-Resistance, *Mater. Lett.*, 2008, **62**, p 2667-2669
13. H.S. Zhang, S. Liao, and X. Dang, Preparation and Thermo-Physical Properties of CeO_2 doped $Gd_2Ce_2O_7$ and $(Gd_{0.9}Ca_{0.1})_2Ce_2O_{6.9}$ Ceramics for Thermal Barrier Coatings, *J. Alloys Compd.*, 2011, **509**, p 1226-1230
14. H.M. Zhou, D.Q. Yi, Z.M. Yu, and L.R. Xiao, Preparation and Thermo-Physical Properties of CeO_2 Doped $La_2Zr_2O_7$ Ceramic for Thermal Barrier Coatings, *J. Alloys Compd.*, 2007, **438**, p 217-221
15. J. Wang, S.X. Bai, H. Zhang, and C.R. Zhang, The Structure, Thermal Expansion Coefficient and Sintering Behavior of Nd^{3+}-Doped $La_2Zr_2O_7$ for Thermal Barrier Coating, *J. Alloys Compd.*, 2009, **476**, p 89-91
16. J. Wu, X.Z. Wei, N.P. Padture, P.G. Klemens, M. Gell, E. Garcia, P. Miranzo, and M.I. Osench, Low-Thermal-Conductivity Rare-Earth Zirconates for Potential Thermal-Barrier-Coating Applications, *J. Am. Ceram. Soc.*, 2002, **85**, p 3031-3035
17. U. Schulz, Phase Transformation in EB-PVD Yttria Partially Stabilized Zirconia Thermal Barrier Coatings During Annealing, *J. Am. Ceram. Soc.*, 2000, **83**, p 904-910
18. R. Taylor and J.R. Brandon, Microstructure, Composition and Property Relationships of Plasma-Sprayed Thermal Barrier Coatings, *Surf. Coat. Technol.*, 1992, **50**, p 141-149

19. X. Huang, D.M. Wang, M. Lamontagne, and C. Moreau, Experimental Study of the Thermal Conductivity of Metal Oxides Co-doped Yttria Stabilized Zirconia, *Mater. Sci. Eng. B*, 2008, **149**, p 63-72
20. J. Wu, X.Z. Wei, N.P. Padture, P.G. Klemens, M. Gell, and E. Garcia, Low-Thermal Conductivity Rare-Earth Zirconates for Potential Thermal-Barrier-Coating Applications, *J. Am. Ceram. Soc.*, 2002, **85**, p 3031-3035
21. C. Viazzi, J.P. Bonino, F. Ansart, and A. Barnabé, Structural Study of Metastable Tetragonal YSZ Powders Produced Via A Sol-Gel Route, *J. Alloys Compd.*, 2008, **452**, p 377-383
22. H.F. Liu, S.L. Li, Q.L. Li, and Y.M. Li, Investigation on the Phase Stability, Sintering and Thermal Conductivity of Sc_2O_3-Y_2O_3-ZrO_2 for TBC Application, *Mater. Des.*, 2010, **31**, p 2972-2977
23. H.F. Liu, S.L. Li, Q.L. Li, Y.M. Li, and W.X. Zhou, Microstructure, Phase Stability and Thermal Conductivity of Plasma Sprayed Yb_2O_3, Y_2O_3 Co-Stabilized ZrO_2 Coatings, *Solid State Sci.*, 2011, **13**, p 513-519
24. J. Su, *Rare Earth Chemistry*, Henan Science and Technology, Zhengzhou, 1994, p 202-260
25. X.Q. Cao, *Materials for Thermal Barrier Coatings*, Science, Beijing, 2007, p 18-19